Journal of Solid State Chemistry **145,** 443–451 (1999)
Article ID jssc.1999.8145, available online at http://www.idealibrary.com on IDEAL®

Structural Characterization and Magnetic Order in Phenoxy-Substituted Divalent Metal Phosphonate Langmuir–Blodgett Films

Gail E. Fanucci*, Melissa A. Petruska*, Mark W. Meisel,† and Daniel R. Talham*,[1]

*Department of Chemistry, †Department of Physics, and Center for Ultralow Temperature Research, University of Florida, Gainesville Florida 32611-7200

Received September 1, 1998; in revised form December 30, 1998; accepted January 5, 1999

IN HONOR OF PROFESSOR PETER DAY FRS ON THE OCCASION OF HIS 60TH BIRTHDAY

Metal phosphonate Langmuir–Blodgett (LB) films of an alkoxyphenyl-substituted phosphonic acid (P4A) have been prepared with the divalent metals Mn^{2+} and Cd^{2+}. Structural characterization with infrared spectroscopy, XPS, and X-ray diffraction shows that the films contain the inorganic continuous lattice of known layered solid-state metal phosphonates with formula $M(O_3PR)H_2O$. Magnetic characterization of the Mn-P4 LB film consists of EPR and magnetometry measurements. The Mn-P4 LB film undergoes a transition to a long-range, canted antiferromagnetic state below 14.8 ± 0.2 K and is only the second example of a continuous lattice LB film to exhibit spontaneous magnetization. These results demonstrate that it is possible to prepare metal phosphonate LB films of functionalized organophosphonic acids while retaining both the inorganic continuous lattice structure and magnetic exchange pathways of the known solid-state metal organophosphonates. © 1999 Academic Press

***Key Words*: metal phosphonates; canted antiferromagnet; LB films; manganese phosphonates.**

INTRODUCTION

The Langmuir–Blodgett (LB) technique provides a way to organize molecules on a water surface with subsequent transfer of the monolayer assembly onto a solid support (1–3). Function can be incorporated into either the polar or nonpolar regions of the films, and interest in functionalized LB films includes their potential use in areas such as chemical sensing, molecular electronic devices, and nonlinear optics (2, 3). Although derivatized organic amphiphiles have received tremendous attention to this end, less effort has been spent investigating films where the physical phenomena are derived from metal ions (2, 4, 5), metal complexes (6), or continuous lattice structures (7–9) incorporated into the polar regions of the films. We have recently introduced the concept of continuous lattice LB films by modeling them after transition-metal phosphonates which are known layered extended solids (10,11). LB films based upon the metal phosphonate architecture provide a way to form mixed organic/inorganic assemblies of functionalized phosphonic acids where both components add physical properties (Fig. 1). The strong ionic/covalent bonding of the inorganic continuous network adds substantial stability to the LB films (7). In addition, physical phenomena such as magnetic order can be introduced through the inorganic continuous lattice network (9). At the same time, functionalized organic groups can be introduced, as in conventional LB films (3) to add physical properties such as nonlinear optical responses or molecule-based conductivity.

Metal phosphonate LB films are formed by Y-type deposition of phosphonic acid monolayers compressed on aqueous subphases containing the appropriate metal ions. The inorganic continuous lattice crystallizes when bilayers are formed during the up stroke of the deposition. A variety of metal phosphonate LB films have been formed (7–9,12,13) each possessing a known solid-state metal phosphonate structure type. LB films based on octadecylphosphonic acid (ODPA) with formulas $M^{II}(O_3PR)H_2O$ ($M^{II} = Mn^{2+}$, Cd^{2+}, Co^{2+}, and Mg^{2+}) (9,12), $M^{II}(HO_3PR)_2$ ($M^{II} = Ca^{2+}$ or Ba^{2+}) (9,12), and $Ln^{III}H(O_3PR)_2$ ($Ln^{III} = La^{3+}$, Ce^{3+}, Sm^{3+}, and Gd^{3+}) (12, 13) have been prepared, where the inorganic network has the same structure as the analogous solid-state metal phosphonate of the same formula (10, 14–17). The manganese octadecylphosphonate, $Mn(O_3PC_{18}H_{37})H_2O$, film was the first example of a magnetic LB film showing spontaneous magnetization and magnetic memory effects below the magnetic ordering temperature of 13.8 K (9).

This article describes metal phosphonate LB films based on 4-(4′-tetradecyloxyphenyl) butylphosphonic acid (P4A, **1**) that form with the $M^{II}(O_3PR)H_2O$ two-dimensional

[1] To whom correspondence should be addressed. E-mail: talham@chem.ufl.edu.

0022-4596/99 $30.00

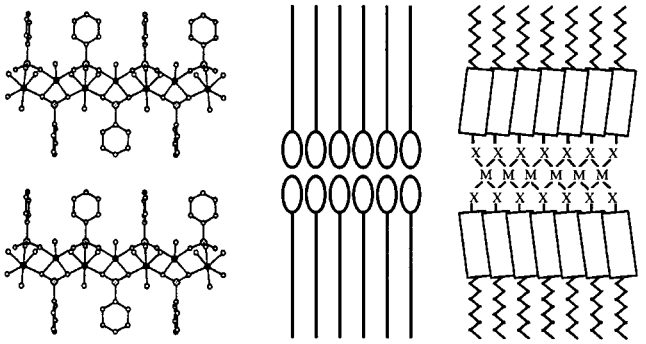

FIG. 1. Comparison of "dual-network" metal phosphonate LB films to polycrystalline metal phosphonate solids. (left) Layered structure of manganese phenylphosphonate (crystallographic data are taken from Ref. 10). (center) Representation of a Y-type LB film, where the balls and sticks represent the polar and nonpolar regions, respectively. (right) A dual-network functionalized metal organophosphonate LB film containing a 2D metal phosphonate continuous lattice in the polar region and a molecular solid network in the nonpolar region.

continuous lattice structure (M^{II} = Mn or Cd), and the magnetic properties of the manganese film are reported. These films are referred to as Mn-P4 and Cd-P4, where the P represents an alkoxyphenyl group and the 4 indicates the number of carbons separating the aryl group from the phosphonate head group. Although the alkoxyphenyl substituent does not add any interesting optical or conducting properties, it can be used to study whether larger organic groups can be organized within LB films while maintaining the divalent metal phosphonate lattice framework and to investigate how the larger organic group affects the magnetic interactions in the layered manganese phosphonate network. Structural characterization consists of X-ray diffraction (XRD), X-ray photoelectron spectroscopy (XPS), and Fourier transform infrared (FTIR) spectroscopy measurements, and the magnetic properties of the Mn-P4 LB film were investigated by electron spin resonance (ESR) and static magnetometry measurements. The Mn-P4 film is shown to be only the second example of an LB film exhibiting spontaneous magnetization. Results show that it is possible to incorporate the alkoxyphenyl group within the divalent metal phosphonate LB film without disruption of the inorganic network or the magnetic exchange pathways.

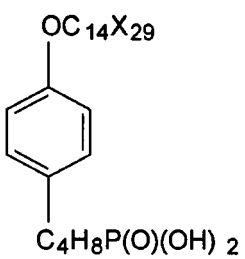

1 (P4A) X = H

2 (*d*P4A) X = D

EXPERIMENTAL

Materials Used

4-(4′-Tetradecyloxyphenyl) butylphosphonic acid (P4A, **1**) and 4-(4′-d_{29}-tetradecyloxyphenyl) butylphosphonic acid (*d*P4A, **2**) were prepared as described in a previous report (18). Octadecyltrichlorosilane (OTS, $C_{18}H_{37}SiCl_3$, 95%) was purchased from Aldrich (Milwaukee, WI) and stored under nitrogen. $MnCl_2 \cdot 6H_2O$ (99.6%) and $CdCl_2 \cdot 5/2H_2O$ (99.7%) were purchased from Fisher Scientific (Pittsburgh, PA) and used as received. A Barnstead NANOpure purification system produced water with an average resistivity of 18 MΩ cm for all experiments.

Substrate Preparation

Single-crystal (1 0 0) silicon wafers were purchased from Semiconductor Processing Company (Boston, MA) and were used as deposition substrates for XPS measurements. Samples for XRD studies were deposited onto glass petrograph slides that were purchased from Beuhler, Ltd. (Lake Bluff, IL). Silicon and glass substrates were cleaned using the RCA cleaning procedure (19) and dried under N_2. Germanium attenuated-total-reflectance (ATR) parallelograms (45°, 50 × 10 × 3 mm), were purchased from Wilmad Glass (Buena, NJ) and were used as substrates for ATR–FTIR experiments. Germanium ATR crystals were cleaned by an oxygen plasma etch and washed with chloroform in a Soxhlet extractor before use. These substrates were made hydrophobic by deposition of a monolayer of OTS (20,21). Mylar sheets (Dupont, DE) were coated with 5 bilayers of calcium arachidate to improve the hydrophobicity of the surface and were used as substrates for ESR and magnetization measurements.

Instrumentation

The LB experiments were performed using modified KSV 5000 and 3000 Instruments (Stratford, CT) that are described in detail elsewhere (18). Infrared spectra were recorded with a Mattson Instruments (Madison, WI) Research Series-1 Fourier transform infrared spectrometer using a deuterated triglyceride sulfide (DTGS) detector. A Harrick (Ossining, NY) TMP stage was used for ATR experiments. Polarized ATR–FTIR spectra were taken with s- and p-polarized light. All ATR–FTIR spectra consist of 1000 scans at 4 cm^{-1} resolution. XPS and XRD experiments were performed using conditions described in previous publications (9,18). A 52-bilayer Mn-P4 LB film (26 bilayers per side) was used for ESR measurements. ESR spectra were recorded on a Bruker (Billerica, MA) ER 200D spectrometer modified with a digital signal channel and a digital field controller. Data were collected using a U.S EPR (Clarksville, MD) SPEC300 data acquisition program

and converted to ASCII format using a U.S. EPR (Clarksville, MD) EPRDAP data analysis program. The temperature was controlled by an Oxford Instruments (Whitney, England) ITC 503 temperature controller and an ESR 900 continuous-flow liquid helium cryostat. Magnetization measurements were performed as described in an earlier report of Mn-ODP LB films using a Quantum Design MPMS SQUID magnetometer (9). A gelcap and plastic straw were used as a sample holder during the measurements. The 52-bilayer Mn-P4 LB film sample was prepared and cut into small pieces and oriented in a gelcap. Measurements were performed for orientations parallel and perpendicular to the substrate surface.

RESULTS AND DISCUSSION

Deposition of M^{II}-P4 LB Films

Crystallization of the metal phosphonate lattice in organophosphonate LB films depends strongly upon the subphase pH (12). If the pH is too low, the metal phosphonate continuous lattice does not form in the transferred LB films. If the subphase pH is too high, the metal ions cross-link the phosphonate head groups on the water surface and the Langmuir monolayer becomes too rigid to transfer. The interactions between the metal ions and the monolayer of P4 can be seen in pressure vs area compression isotherms measured as a function of subphase pH. At low pH, the isotherm closely resembles that of P4 on a pure water subphase (18), indicating that the metal ions do not interact with the phosphonate head groups. This point is illustrated in Fig. 2 for a subphase containing Mn^{+2}, where at pH 3.0 the monolayer collapses at an area of 25 $Å^2$/molecule with a collapse pressure of 69 mN/m. As the pH is increased to 4.0, the collapse pressure decreases and the compression isotherm becomes less steep, indicating that the metal ions are beginning to associate with the monolayer. Above pH 4.4, the shape of the isotherm indicates that the monolayer has become rigid as a result of cross-linking of the phosphonate head groups by the metal ions. Almost identical behavior was observed for monolayers of P4A on 0.5 mM Cd^{2+} subphases as a function of pH, and no differences were observed in compression isotherms of *d*P4A.

Isotherms such as those shown in Fig. 2 are used to estimate the subphase pH where quality metal phosphonate LB bilayers are deposited. By "quality" bilayer we mean complete transfer from the water surface to the solid substrate on both the down stroke and up stroke of the deposition process with complete formation of the metal phosphonate continuous lattice within the polar headgroup region of the film. From Fig. 2, the optimum subphase pH range (12) to deposit quality bilayers of P4 with manganese ions is pH 4.0–4.4. This pH range is also optimum for the deposition of Cd-P4 LB films. M^{II}-P4 LB films are transferred onto a solid support by compressing the Langmuir monolayer to a surface pressure of 25 mN/m, letting the film stabilize for 3–5 min, and then lowering the hydrophobic substrate through the film at a speed of 3 mm/min. The substrate is then raised through the compressed monolayer at a speed of 1 mm/min, thereby completing a head-to-head bilayer. The slower deposition speed on the up stroke allows for the draining of excess subphase and the crystallization of the inorganic lattice. However, even within the optimum pH range, the monolayers of P4 become too rigid to transfer after an extended time period. This gradual increase in film rigidity prevents the continuous deposition of multilayer samples and has been observed for other metal phosphonate LB films (9). Consequently, after the deposition of one bilayer, the monolayer is removed from the water surface, and a new monolayer is spread. Repeated deposition results in multilayer assemblies.

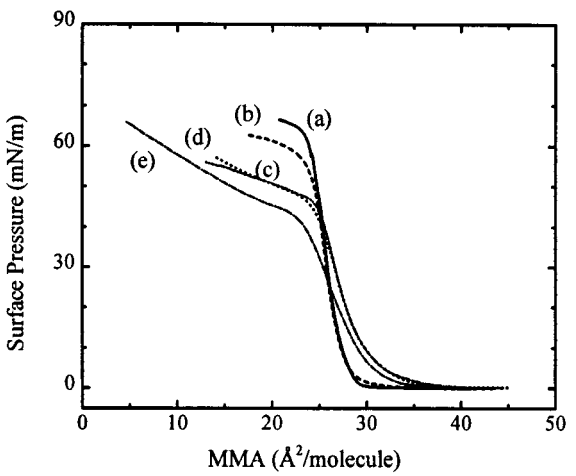

FIG. 2. Pressure vs mean molecular area (MMA) isotherms of P4A **(1)** on 0.5 mM Mn^{2+} subphases at pH (a) 3.0, (b) 3.5, (c) 4.0, (d) 4.4, and (e) 4.7.

Structural Characterization

XRD demonstrates that each of the M^{II}-P4 films is layered. Four orders of (0 0 *l*) Bragg reflections ($l = 2$–5) are observed for both M^{II}-P4 samples, where each sample consists of 10 bilayers. A bilayer thickness of 51 $\pm$ 1 Å is found for both LB films. XPS is used to determine the metal: phosphorus stoichiometry in the films. Table 1 lists the relative areas of the observed P_{2p} and M^{II} ($Mn_{2p3/2}$, $Cd_{3d5/2}$) photoelectron peaks in single bilayers of M^{II}-P4. The values are determined by integrating the areas of the P_{2p} and the corresponding M^{II} peaks and accounting for instrumental sensitivity factors (22–24). The solid-state divalent metal phosphonate materials of formula $M^{II}(O_3PR)H_2O$ have a 1:1 metal:phosphorus stoichiometry, and the observed XPS areas are within 5% of those expected (calculated values in Table 1) for this structure assuming a layered film

TABLE 1
Bilayer Thickness[a] and Relative Intensities[b] of Phosphorus and Metal XPS Peaks for M^{II}-P4 LB Films

	Bilayer thickness		XPS observed relative intensity		XPS calculated relative intensity[d]	
M^{II}-P4 LB	Experimental ($\pm$ 1 Å)	Calculated[c]	%P ($\pm$ 3%)	%M ($\pm$ 3%)	%P ($\pm$ 2%)	%M ($\pm$ 2%)
Mn	51	49–53	63	37	60	40
Cd	51	48–52	49	51	47	53

[a] Bilayer thicknesses are determined from XRD patterns of samples comprising 10 bilayers.
[b] Integrated areas are corrected for instrument and atomic sensitivity factors. The following photoelectron peaks were used: P_{2p} (134.5 eV), $Cd_{3d5/2}$ (406.7 eV), $Mn_{2p3/2}$ (643 eV).
[c] Calculated thicknesses were determined as described in the text.
[d] Values are calculated assuming a 1 : 1 metal : phosphorous stoichiometry and using a procedure discussed in previous publications (Ref. 28).

geometry (25–29). The close agreement between the observed relative percentages and the calculated percentages indicates a phosphorus : metal stoichiometry of 1 : 1 in the M^{II}-P4 LB films, and this ratio is consistent with the structure of the solid-state compounds.

It has previously been shown that the phosphonate (P–O) infrared stretching modes can be used to correlate the metal–phosphonate continuous lattice structures of LB films with those of the solid-state structures (9). The P–O stretching frequencies are very sensitive to the mode of metal bonding (9,12,13,30), and the different metal phosphonate structure types give distinct P–O stretching patterns in their IR spectra. Figure 3 shows the asymmetric phosphonate ($\nu_a(PO_3^{2-})$) and symmetric phosphonate ($\nu_s(PO_3^{2-})$) stretches, occurring at 1083.9 and 978.8 cm^{-1} for the Mn-P4 LB film and at 1084.9 and 958.6 cm^{-1} for the Cd-P4 film, respectively. The shape, relative intensity, and frequency of these modes are almost identical to those of $Mn(O_3PC_2H_4)H_2O$ and $Cd(O_3PC_2H_4)H_2O$ solid-state samples (Table 2). This similarity indicates that the M^{II}-P4 LB films contain the same 2D metal phosphonate continuous lattice of the analogous $M(O_3PR)H_2O$ solid-state compounds (9). In addition, the IR mode at 1608 cm^{-1} in the spectra of both films corresponds to the H–O–H bending mode of the coordinated water molecule present in the $M(O_3PR)$ H_2O structure, which also occurs at 1608 cm^{-1} in spectra of the solids.

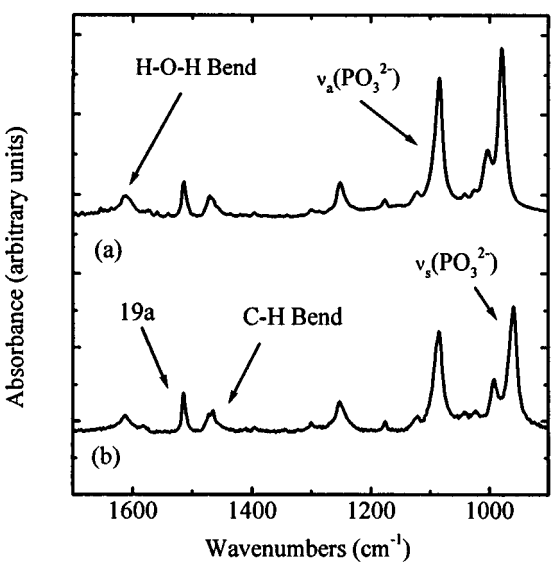

FIG. 3. ATR–FTIR spectra of 5 bilayers of (a) Mn-P4 and (b) Cd-P4 LB films. Peak assignments are discussed in the text.

Figure 4 shows ATR–FTIR spectra from 4000 to 950 cm^{-1} of 10-bilayer samples of both Mn-P4 and the partially deuterated Mn-dP4 with labeled peaks corresponding to the asymmetric methylene ($\nu_a(CH_2)$ and $\nu_a(CD_2)$) and the symmetric methylene ($\nu_s(CH_2)$ and $\nu_s(CD_2)$) stretching vibrations, and to the 19a C–C phenyl skeletal deformation (31). A linear increase in the intensity of $\nu_a(CH_2)$ and mode 19a as a function of the number of bilayers (Fig. 5A) shows that the same amount of P4 is transferred during each deposition cycle. In addition, a linear increase in the intensity of $\nu_a(PO_3^{2-})$ and the H–O–H bending mode (Fig. 5B) shows that the metal phosphonate continuous lattice structure is maintained in the multilayer films.

TABLE 2
Phosphonate Stretching Frequencies of Divalent Metal Alkylphosphonate Powders[a] and M^{II}-P4 LB Films[b]

Sample	$V_a(PO_3^{2-})$ (cm^{-1})	$V_s(PO_3^{2-})$ (cm^{-1})
Mn-P4 LB Film	1084	979
$Mn(O_3PC_2H_5)H_2O$ Powder	1087	988/964
Cd-P4 LB Film	1085	959
$Cd(O_3PC_2H_5)H_2O$ Powder	1089	957

[a] Powder samples were measured as KBr pellets.
[b] LB films were deposited onto Ge ATR crystals for IR measurements.

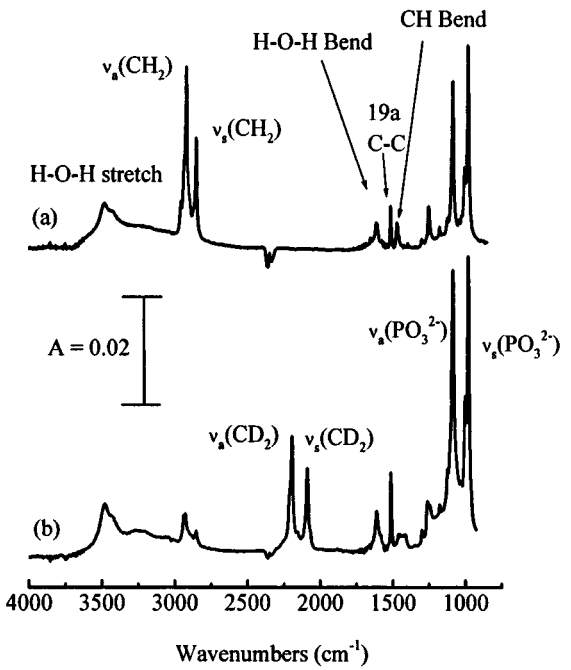

FIG. 4. ATR–FTIR spectra of 10 bilayers of (a) Mn-P4 and (b) Mn-*d*P4 showing the IR modes originating from the separate hydrogenated 4-carbon and perdeuterated 14-carbon segments. Peak assignments are discussed in the text.

The position and shape of the aliphatic CH stretching modes in the IR spectra of monolayer and multilayer films reflect the conformational order and packing of the aliphatic chains (21, 32, 33). In particular, the frequency of $\nu_a(CH_2)$ reflects the conformational order of the alkyl chains, and the full-width-at-half-maximum (fwhm) of this vibrational mode is a measure of the degree to which the alkyl chains are closed-packed. The spectrum in Fig. 4 of Mn-*d*P4 differentiates the signals arising from the separate 4-carbon and 14-carbon segments of the organophosphonate (where the 14-carbon segment is perdeuterated). The $\nu_a(CD_2)$ and $\nu_s(CD_2)$ stretches occur at 2193 and 2090 cm^{-1}, respectively, for both the Mn- and Cd-*d*P4 LB films. The bands are narrow with fwhm values of 20 cm^{-1}. The frequency and shape of the bands are similar to those observed in spectra of a KBr pellet of *d*P4A and indicate that the 14-carbon chains are closed-packed and arranged in an all-trans conformation (18). In each case, the C–H modes originating from the 4-carbon segment closely resemble the C–H modes observed in solid-state spectra of butylphosphonic acid, although, we are unable to comment on the arrangement of the 4-carbon segment since the correlation of stretching frequency with organization of the alkyl groups is less meaningful for short chains (32, 34).

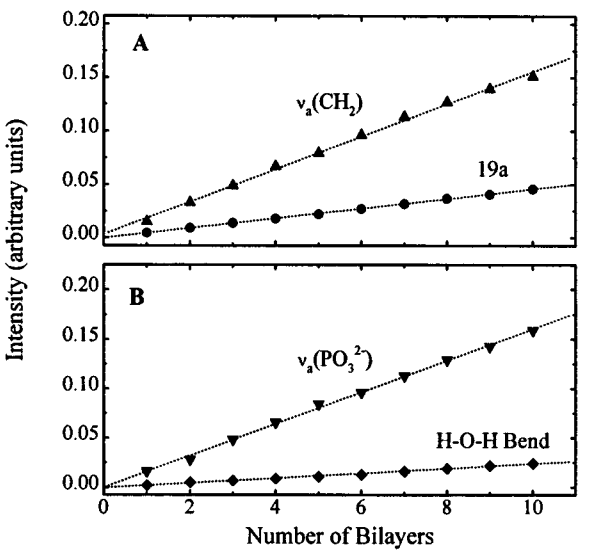

FIG. 5. Integrated intensity of (A) the $V_a(CH_2)$ and 19a FTIR absorptions and (B) the $V_a(PO_3^{2-})$ and H–O–H bend FTIR absorptions as a function of the number of bilayers of the Mn-P4 LB film. A linear relationship in (A) shows that the same amount of film transfers during each deposition while in (B) it further indicates that the metal phosphonate continuous lattice structure is maintained throughout the repeated deposition procedure.

The tilt angles of the 14-carbon chain axes and of the phenyl moieties in M^{II}-*d*P4 LB films were determined from polarized ATR–FTIR experiments. Detailed accounts of this procedure have been described by other authors (35–38). The dichroic ratios, defined as $D = (A_x + A_z)/(A_y)$, of the $\nu_a(CD_2)$ stretching vibration and 19*a* C– C phenyl skeletal deformation, as well as the corresponding tilt angles, are listed in Table 3. In each case, the phenyl moiety is tilted at an angle of $23 \pm 2^\circ$ from the surface normal. The measured dichroic ratios of the $\nu_a(CD_2)$ for both the Mn- and Cd-*d*P4 films correspond to a tilt angle of $47 \pm 3^\circ$ from the surface normal for the 14-carbon chain.

The measured tilt angles can be used to compare the molecular orientation in the film to the bilayer thickness determined from XRD measurements. To calculate the length of each molecule, the following distances were used (18): 1.2 Å for the length of each CH_2–CH_2 unit on an

TABLE 3
Dichroic Ratios[a], *D*, and Corresponding Molecular Axis[b] Tilt Angles for M^{II}-P4 LB Films

Sample	Mode	Frequency (cm^{-1})	*D*	Tilt angle (deg)
Mn-P4	$V_a(CH_2)$	2193	1.30 ± 0.05	48 ± 4
	C=C 19a	1515	2.6 ± 0.1	24 ± 2
Cd-P4	$V_a(CH_2)$	2193	1.33 ± 0.05	48 ± 4
	C=C 19a	1515	2.7 ± 0.1	23 ± 2

[a] Dichroic ratio, *D*, is defined as $(A_x + A_z)/(A_y)$.

[b] Molecular axes are defined along the C1–C4 axis of the phenyl moiety and at 90° to the methylene bonds for the alkyl-chains. Tilt angles are defined with respect to the film normal (0°).

all-trans alkyl chain, 1.2 Å for the C(alkyl)–O bond length, 5.4 Å for the phenoxy moiety, 3 Å for the van der Waals gap between the adjacent tails in the bilayer, and 4.5 Å for the P–O–*M*–O–P distance (determined from crystallographic data in Ref 10). The calculated distances (Table 1) are reported as a range because the tilt angle of the 4-carbon segment is unknown and disorder is expected. The upper and lower values in the range are those obtained when the C4 segment has its maximum length (tilt angle of 0°) and when it is oriented at a tilt angle of 47.3° (equal to that of the 14-carbon segment), respectively. The calculated range of 48–53 Å corresponds well with the bilayer thickness of 51 ± 1 Å determined from XRD measurements.

The structural characterization confirms that quality LB films of P4 can be prepared with manganese and cadmium ions. The quality of the films is maintained when multiple bilayers are deposited. The inorganic lattice within each bilayer adopts the $M(O_3PR)H_2O$ structure of the solid-state manganese and cadmium phosphonates. The organic molecules are well-organized with the phenyl groups oriented nearly upright with respect to the metal ion plane, and the 14-carbon alkyl tails tilt to achieve close packing within the spacing constraints imposed by the phenoxy groups and the metal phosphonate lattice. Magnetic measurements further confirm that the continuous lattice LB films are isostructural with the solid-state phosphonates.

Magnetic Properties

ESR measurements were made on a 52-bilayer Mn-P4 LB film sample that was cut into thin strips, stacked, and placed vertically into a conventional ESR tube such that the LB plane could be rotated with respect to the applied magnetic field. The inset in Fig. 6 shows a representative ESR signal from the Mn-P4 LB film. The signal is dipolar broadened, characteristic of an exchange-coupled lattice, and no hyperfine Mn^{2+} splittings are observed. Figure 6 shows the peak-to-peak line width, ΔH_{p-p}, of the ESR signal at room temperature as a function of orientation (39). The direction normal to the LB planes is defined as 0°. The line width has a maximum value of 264 G at 0° and 180° with a minimum value of 208 G at 55° and 125°. Within experimental error, the *g* value does not change as a function of orientation and is consistently found to be 1.99 ± 0.02. The data in Fig. 6 are fit with the expression, $\Delta H_{p-p} = A + B(3\cos^2\phi - 1)^2$, which is characteristic of a two-dimensional (2D) spin system with antiferromagnetic Heisenberg exchange (40–42). The fit yields values of $A = 208$ and $B = 16$, where A and B encompass contributions to the line width from both exchange and dipolar interactions. The important result from Fig. 6 is the observation of 2D magnetic exchange within the layers (43,44).

The peak-to-peak line width as a function of temperature for a sample aligned perpendicular to the magnetic field is shown in Fig. 7. The line width is nearly constant as the temperature is lowered until a significant broadening occurs below 50 K. From 50–18 K, the line width increases rapidly until the signal becomes so broad that it can no longer be detected. This broadening also occurs in the Mn–ODP LB film (43,44) and in polycrystalline solid-state manganese alkylphosphonates (45–47), and results from antiferromagnetic fluctuations that signal an approaching magnetic ordering transition. The magnetic resonance signals from the

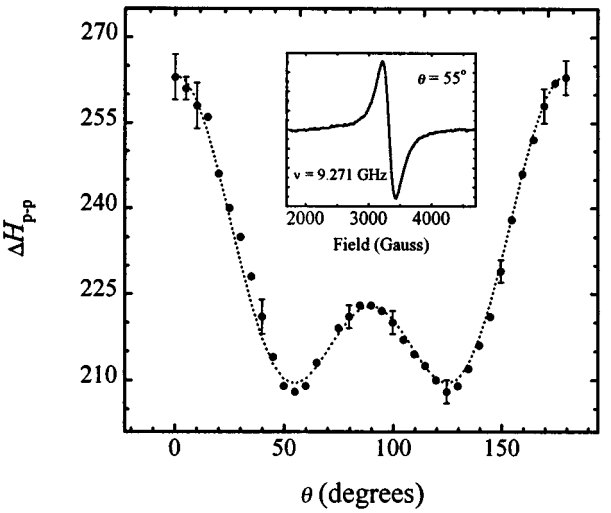

FIG. 6. Room-temperature ESR line width as a function of orientation for a 52-bilayer Mn-P4 LB film. The dotted line is a fit to the data and is discussed in the text. The direction normal to the LB planes is defined as 0°. The inset shows, as an example, the EPR signal at $\theta = 55°$.

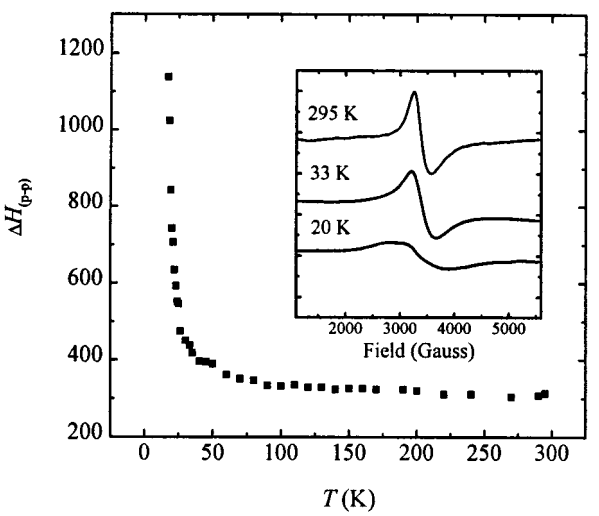

FIG. 7. ESR line width as a function of temperature for the Mn-P4 LB film oriented 0° with respect to the magnetic field. The experimental uncertainties are given by the size of the data points. The inset gives examples of the ESR signal at 295, 33, and 20 K. The significant broadening of the line below 50 K is characteristic of an approaching magnetic ordering transition.

ordered state (the antiferromagnetic resonances (48,49)) are not observed because, for the manganese phosphonates, they occur outside the frequency and field range accessible by an X-band ESR spectrometer (49).

The integrated area of an isotropic Lorentzian signal is proportional to the spin susceptibility (40), and a plot of the area of the ESR signal as a function of temperature is shown in Fig. 8. The solid line is a fit of the data using a series expansion solution for a 2D quadratic lattice of $S = 5/2$ spins with Heisenberg nearest-neighbor exchange (41). The fit further illustrates that at high temperatures the magnetic exchange exists within the layers of manganese ions and that the exchange interaction is isotropic. The strength of the magnetic interaction is given by the value of the exchange constant, $J = -2.7 \pm 0.1$ K, which was determined from this fit. An estimate of J can also be determined from the temperature of the susceptibility maximum (50) by $kT\chi_{max}/|J| = 2.05S(S+1)$. From Fig. 8, $T\chi_{max}$ occurs at 25 K, leading to a value of $J = -2.8 \pm 0.1$ K which is in close agreement with the value obtained from fitting the temperature dependent data. The data can also be viewed as a Curie–Weiss plot, and the inset in Fig. 8 shows a plot of 1/area vs temperature, where the x-axis intercept of $-58 \pm 2^\circ$ provides a value for the Weiss constant, θ. The magnetic exchange parameters of J and θ of the Mn-P4 LB film are similar in value to those of the bulk phosphonate solids (45–47), adding further evidence that the in-plane Mn–O–Mn interactions are the same as those of the solid-state materials.

Although the magnetically ordered state cannot be probed by X-band ESR spectroscopy, evidence for an ordered state is observed in magnetometry measurements. The analogous solid-state metal phosphonates are known to undergo transitions to an ordered state with a weak ferromagnetic moment due to incomplete cancellation of the spins that results from canting of the antiferromagnetically coupled sublattice moments (45,46). Such systems are referred to as canted antiferromagnets or weak ferromagnets (50). An up-turn in the temperature-dependent magnetic susceptibility observed at $T < T\chi_{max}$ is a signature of canted antiferromagnetic ordering (50,51), with T_N being the temperature at which the up-turn occurs. For such materials, a nonzero magnetization, or weak ferromagnetic moment, can be observed at temperatures below T_N in difference plots of the field-cooled (FC) and zero field-cooled (ZFC) temperature-dependent magnetization, ΔM_{FC-ZFC}. Figure 9 shows a plot of ΔM_{FC-ZFC} vs temperature for the Mn-P4 film oriented with the planes parallel to the applied magnetic field. The significantly nonzero ΔM below T_N is evidence for a transition to long-range magnetic order with spontaneous magnetization and is consistent with a transition to a canted antiferromagnetic state. The ZFC data in the perpendicular orientation (Fig. 10) show that the film orders at $14.8 \pm$

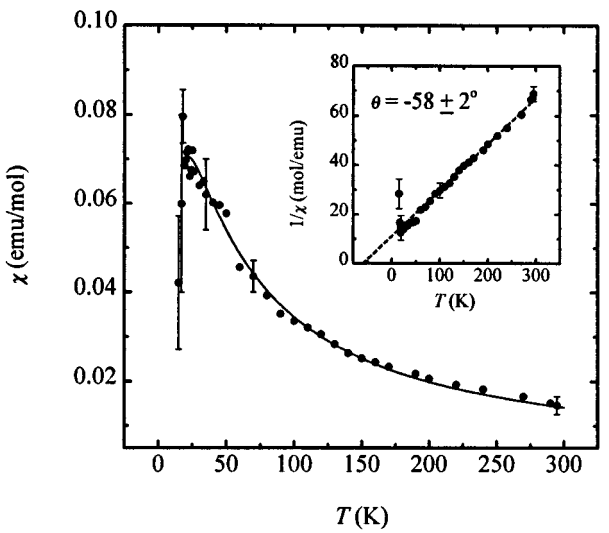

FIG. 8. Temperature dependence of the integrated area (normalized to the room temperature spin- only susceptibility value) of the ESR signal of the Mn-P4 LB film. The solid line is a fit to the data using a model described in the text for a two-dimensional lattice of Mn^{2+} $S = 5/2$ ions with Heisenberg antiferromagnetic exchange with exchange constant $J = -2.7$ K. The inset shows a plot of the inverse area vs temperature, and the dotted line is a fit to the Curie–Weiss law for $T > 80$ K, giving a Weiss constant of $\theta = -58$ K, indicating antiferromagnetic exchange.

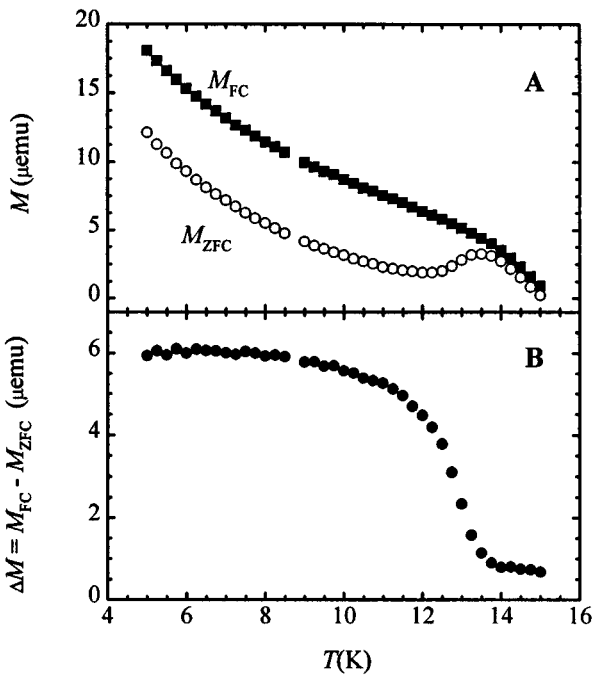

FIG. 9. Magnetization vs temperature for the 52-bilayer Mn-P4 LB film with the measuring field applied parallel to the plane of the film. (A) Comparison of the magnetization data taken upon warming the film after cooling in zero-applied field (M_{ZFC}) and cooling in a field of 0.1 T (M_{FC}). In both cases, the measuring field is 0.01 T. (B) The difference in the FC and ZFC magnetization, ΔM_{FC-ZFC}, shows spontaneous magnetization below T_N. The spontaneous magnetization is evidence for a transition to a canted antiferromagnetic state.

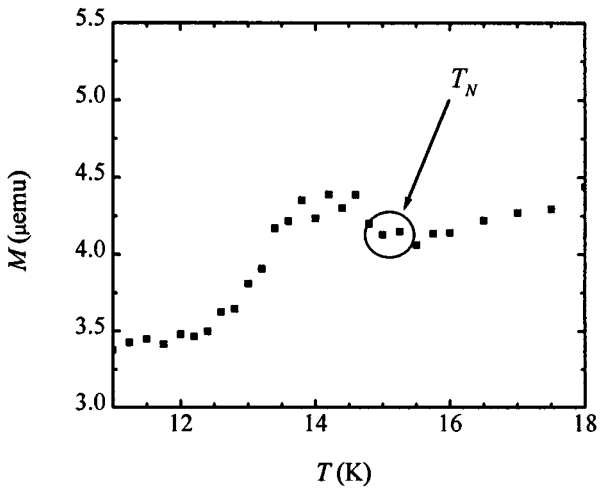

FIG. 10. Zero-field cooled magnetization data, M_{ZFC}, for the Mn-P4 LB film oriented perpendicular to the LB planes. The ordering temperature, $T_N = 14.8 \pm 0.214$ K, is indicated by an up turn in the data, which is characteristic of canted antiferromagnetic ordering.

0.2 K. The net moment is larger in the parallel orientation, indicating that the magnetic easy axis is perpendicular to the plane and that the canted moment lies within the metal planes. The nonzero magnetization perpendicular to the metal planes can arise from imperfect alignment of the sample or from uncompensated spins at the magnetic domain boundaries. A spin–flop (50) transition near 2.5 T is observed in the magnetization versus field data when the applied field is perpendicular to the metal planes, further indicating that the magnetic easy-axis lies normal to the film surface. These findings are consistent with the spin arrangement found for the Mn-ODP LB film (9) and for the analogous manganese phosphonate solid compounds (45,46,52,53).

The Mn-P4 film is the second example of a magnetic LB film that contains the manganese phosphonate lattice structure and exhibits spontaneous magnetization. The magnetometry measurements show that the Mn-P4 film orders to a canted antiferromagnetic state and that the alkoxyphenyl moieties do not disrupt the Mn–O–Mn exchange pathways of the solid-state $Mn(O_3PR)H_2O$ network. Interestingly, the ordering temperature of the Mn-P4 film, $T_N = 14.8 \pm 0.2$ K, is higher than the, $T_N = 13.8 \pm 0.2$ K determined for the Mn-ODP LB film (9) and is comparable to that of polycrystalline manganese butylphosphonate, where $T_N = 15.0 \pm 0.2$ K (45,46). In the solid-state alkylphosphonates, T_N varies slightly as the alkyl group changes, possibly reflecting subtle changes in the metal–phosphonate bonding geometry. It may be that the 4-carbon tether in P4 results in metal–oxygen–phosphorus bonding more like that found in the short chain alkylphosphonates than in the longer chain analogs such as manganese hexylphosphonate (49) ($T_N = 14.1 \pm 0.2$ K) and the Mn-ODP LB film. Finally, the ordering temperatures permit comment on the magnetic and, therefore, structural coherence lengths in the LB films. For a 2D spin system, the magnetic coherence length diverges as $T \to T_N$ (40). Diminished coherence lengths, caused by either impurities or small domain sizes, will suppress T_N relative to the infinite solid. The observation that T_N in both the Mn-P4 and Mn-ODP LB films are comparable to solid-state analogs suggests that the ordering temperatures are not limied by the size of the domains within the films.

CONCLUSIONS

This study demonstrates that metal phosphonate continuous lattice LB films of a phenoxy substituted organophosphonic acid can be formed with either Mn^{2+} or Cd^{2+} metals. Films of Mn-P4 and Cd-P4 possess the metal–oxygen–phosphorus bonding geometry of the known solid-state metal phosphonates with formula $M^{II}(O_3PR)H_2O$, where M^{II} = Mn or Cd. Inclusion of the aryl group into the nonpolar regions of these films does not disrupt the bonding geometry of the metal phosphonate lattice, and magnetic studies of the Mn-P4 LB film show that the magnetic exchange interactions in this sample are similar to those of the analogous polycrystalline manganese phosphonates. The Mn-P4 LB film is shown to be the second example of a continuous lattice LB film to undergo a transition to long-range magnetic order.

ACKNOWLEDGMENTS

The authors acknowledge the National Science foundation for financial support and Prof. J.R. Childress for making the SQUID magnetometer available for our use (acquired though a NSF instrumentation grant, No. DMR-9422192). M.A.P. thanks the National Science Foundation for a predoctoral fellowship. Special thanks are given to the Florida Major Analytical Instrumentation Center for use of XRD and XPS facilities.

REREFENCES

1. K. B. Blodgett, *J. Am. Chem. Soc.* **57,** 1007 (1935).
2. G. G. Roberts, "Langmuir–Blodgett Films." Plenum Press, New York, 1990.
3. A. Ulman, "An Introduction to Ultrathin Organic Films: From Langmuir–Blodgett to Self-Assembly." Academic Press, Boston, 1991.
4. M. Pomerantz, "Studies of Literally Two-Dimensional Magnets of Manganese Stearate NATO ASI Series—Phase Transitions in Surface Films" (J. G. Dash and J. Ruvalds, Eds.), p. 317. Plenum, New York, 1980.
5. M. Pomerantz and R. A. Pollak, *Chem. Phys. Lett.* **31,** 602 (1975).
6. M. Clement-Leon, C. Mingotaud, B. Agricole, C. Gomez-Garcia, E. Coronado, and P. Delhaes, *Angew. Chem., Int. Ed. Engl.* **36,** 1114 (1997).
7. H. Byrd, J. K. Pike, and D. R. Talham, *Chem. Mater.* **5,** 709 (1993).
8. H. Byrd, S. Whipps, J. K. Pike, J. Ma, S. E. Nagler, and D. R. Talham, *J. Am. Chem. Soc.* **116,** 295 (1994).

9. C. T. Seip, G. E.Granroth, M. W. Meisel, and D. R. Talham, *J. Am. Chem. Soc.* **119,** 7084 (1997).
10. G. Cao, H. Lee, V. M. Lynch, and T. E. Mallouk, *Inorg. Chem.* **27,** 2781 (1988).
11. G. Cao, H.-G. Hong, and T. E. Mallouk, *Acc. Chem. Res.* **25,** 420 (1992).
12. G. E. Fanucci, C. T. Seip, M. A. Petruska, S. Ravaine, C. M. Nixon, and D. R. Talham, *Thin Solid Films* **327–329,** 131 (1998).
13. G. E. Fanucci and D. R. Talham, *Langmuir* (1999) in press.
14. G. Cao, H. Lee, V. M. Lynch, and T. E. Mallouk, *Solid State Ionics* **26,** 63 (1988).
15. G. Cao, V. M. Lynch, J. S. Swinnea, and T. E. Mallouk, *Inorg. Chem.* **29,** 2112 (1990).
16. D. M. Poojary, B. Zhang, A. Cabeza, M. A. G. Aranda, S. Bruque, and A. Clearfield, *J. Mater. Chem.* **6,** 639 (1996).
17. R.-C. Wang, Y. Zhang, H. Hu, R. R. Frausto, and A. Clearfield, *Chem. Mater.* **4,** 864 (1992).
18. M. A. Petruska, G. E. Fanucci, and D. R. Talham, *Chem. Mater.* **10,** 177 (1998).
19. W. Kern, *J. Electrochem. Soc.* **137,** 1887 (1990).
20. L. Netzer and J. Sagiv, *J. Am. Chem. Soc.* **105,** 674 (1983).
21. R. Maoz and J. Sagiv, *J. Colloid Interface Sci.* **100,** 465 (1984).
22. C. D. Wagner, L. E. Davis, M. V. Zeller, J. A. Taylor, R. M. Raymond, and L. H. Gale, *Surf. Interface Anal.* **3,** 211 (1981).
23. "5000 Series ESCA Systems Version 2.0 Instruction Manual." Perkin–Elmer Physical Electronics Division, Eden Prairie, MN, 1989.
24. "Perkin–Elmer Handbook of X-Ray Photoelectron Spectroscopy." Perkin–Elmer Physical Electronics Division, Eden Prairie, MN, 1994.
25. M. P. Seah and W. A. Dench, *Surf. Interface Anal.* **1,** 1 (1979).
26. C. R. Brundle, H. Hopster, and J. D. Swalen, *J. Chem. Phys.* **70,** 5190 (1979).
27. S. Akhter, H. Lee, H.-G. Hong, T. E. Mallouk, and J. M. White, *J. Vac. Sci. Technol.* **7,** 1608 (1989).
28. J. K. Pike, H. Byrd, A. A. Morrone, and D. R. Talham, *Chem. Mater.* **6,** 1757 (1994).
29. The calculated relative XPS areas include corrections for differences in the photoelectron escape depths (see Ref. 28).
30. B. L. Frey, D. G. Hanken, and R. M. Corn, *Langmuir* **9,** 1815 (1993).
31. G. Varsanyi, "Vibrational Spectra of Benzene Derivatives." Academic, New York, 1969.
32. M. D. Porter, T. B. Bright, D. L. Allara, and C. E. D. Chidsey, *J. Am. Chem. Soc.* **109,** 3559 (1987).
33. K. A. Wood, R. G. Snyder, and H. L. Strauss, *J. Chem. Phys.* **91,** 5255 (1989).
34. R. G. Snyder, H. L. Strauss, and C. A. Elliger, *J. Phys. Chem.* **86,** 5145 (1982).
35. N. Tillman, A. Ulman, J. S. Schildkraut, and T. L. Penner, *J. Am. Chem. Soc.* **110,** 6136 (1988).
36. V. Cammarata, L. Atanasoska, L. L. Miller, C. J. Kolaskie, and B. J. Stallman, *Langmuir* **8,** 876 (1992).
37. G. L. Haller and R. W. Rice, *J. Phys. Chem.* **74,** 4386 (1970).
38. W.-H. Jang and J. D. Miller, *J. Phys. Chem.* **99,** 10272 (1995).
39. Note that the LB film sample has a common axis normal to the surface since the layers are deposited parallel to the substrate, but the in-pane direction consists of a distribution of circularly averaged domains.
40. L. J. de Jongh, "Magnetic Properties of Layered Transition Metal Compounds." Kluwer Academic, Dordrecht, 1990.
41. M. E. Lines, *J. Phys. Chem. Solids* **31,** 101 (1970).
42. D. Gatteschi, and R. Sessoli, *Magn. Res. Rev.* **15,** 1 (1990).
43. H. Byrd, J. K. Pike, and D. R. Talham, *J. Am. Chem. Soc.* **116,** 7903 (1994).
44. C. T. Seip, H. Byrd, and D. R. Talham, *Inorg. Chem.* **35,** 3479 (1996).
45. S. G. Carling, P. Day, D. Visser, and R. K. Kremer, *J. Solid State Chem.* **106,** 111 (1993).
46. S. G. Carling, P. Day, and D. Visser, *J. Phys.: Condens. Matter.* **7,** L109 (1995).
47. J. Le Bideau, C. Payen, B. Bujoli, P. Palvadeau, and J. Rouxel, *J. Magn. Magn. Mater.* **140–144,** 1719 (1995).
48. S. Foner, "Magnetism" (G. T. Rado and H. Suhl, Eds.), Vol. 1, p. 383. Academic Press, New York, 1963.
49. G. E. Fanucci, J. Krzystek, M. W. Meisel, L.-C. Brunel, and D. R. Talham, *J. Am. Chem. Soc.* **120,** 5469 (1998).
50. R. L. Carlin, "Magnetochemistry." Springer-Verlag, Berlin, 1986.
51. T. Moriya, *Phys. Rev.* **120,** 91 (1960).
52. D. Visser, S. G. Carling, P. Day, and J. Deportes, *J. Appl. Phys.* **69,** 6016 (1991).
53. S. G. Carling, P. Day, and D. Visser, *Inorg. Chem.* **34,** 3917 (1995).